Fuel Consumption and Pollutant Emission Optimization at Part and Full Load of a High-Performance V12 SI Engine by a 1D Model

Author, co-author (Do NOT enter this information. It will be pulled from participant tab in MyTechZone)

Affiliation (Do NOT enter this information. It will be pulled from participant tab in MyTechZone)

Abstract

Modern internal combustion engines show complex architectures in order to improve their performance in terms of brake torque and fuel consumption. Concerning naturally-aspirated engines, an optimization of the intake port geometry, together with the selection of a proper valve timing, allow to improve the cylinder filling and hence the performance. The identification of an optimal calibration strategy at test bench usually requires long and expensive experimental activities. Numerical tools can help to support engine calibration, especially in the early design phases.

In the present work, a 12-cylinder naturally aspirated spark ignition engine is investigated. The engine is experimentally tested under full and part load operations. Main performance parameters, in-cylinder pressure cycles and raw pollutant emissions are measured. The engine is schematized in a one-dimensional model (GT-Power™), where "user routines" are employed to simulate turbulence, combustion, knock and pollutant production. 1D model is validated against the experimental data, denoting a good accuracy.

A calibration procedure is implemented by an external optimizer, coupled with the 1D engine model, with the aim of minimizing the fuel consumption. The procedure decision parameters are intake and exhaust valve timings, and combustion phasing. Proper constraints are posed for residual gas fraction and knock intensity. The optimal calibration strategies have been recognized for two operating conditions, where the engine most frequently works along an RDE driving cycles.

Main drivers for engine efficiency are intake de-throttling at part load, thanks to the internal EGR caused by a Miller-Atkinson valve strategy, and cylinder filling maximization at high load. A 'virtual' calibration of the considered engine, employing the developed automatic procedure, is identified on completely theoretical basis. The proposed methodology shows the capability to drive and support the experimental engine calibration and presents the potential to be very helpful in reducing the related costs and time-to-market.

Introduction

Nowadays the efforts aimed at enhancing the Internal Combustion Engines (ICEs) are mainly focused on the fuel consumption minimization to comply with binding CO_2 emission legislation for vehicle homologation [1]. Concerning the Spark-Ignition ICEs, the most widespread path to satisfy the pollutant emission limits is the adoption of a TWC along the exhaust line. As known, this solution poses some issues, such as a low efficiency at cold start or an effectiveness degradation because of aging. In addition, it involves the impossibility to exploit the advantages of lean combustions, since a close-to-stoichiometric air/fuel mixture is mandatory for efficient TWC operation. For the above reasons, a growing interest towards solutions limiting engine raw emissions is emerging.

To face these issues, various techniques have been introduced in order to improve the efficiency, including downsizing [2,3], Variable Valve Actuation/Timing (VVA/VVT) system, variable Compression Ratio (CR) [4-8], external cooled Exhaust Gas Recirculation (EGR) [9-14], water injection [15-17] and pre-chamber ignition devices [18-20]. Referring to the recalled solutions, it is known that they ensure to some improvements in the performance parameters, but this advantages highly depend on the considered operating condition. As an example, the most prevalent techniques for Brake Specific Fuel Consumption (BSFC) advantages at low load above all entail a reduction in the pumping losses (engine downsizing and VVA/VVT) or an increase in the thermodynamic efficiency (high CR). The selection of a high CR may cause the onset of knocking phenomena at medium/high loads. This obliges a delay of the combustion phasing, penalizing the engine efficiency. In addition, an excessive exhaust temperature may occur as well, which leads to need for the air/fuel mixture enrichment, with further fuel consumption penalizations. A breakthrough, solving simultaneously the above concerns, seems to be the pre-chamber system, which allows ultra-lean combustions and reduced pollutant emissions. However, its application in a commercial engine is still to come because of issues related to high costs and control complexity.

Concerning more common architectures of naturally aspirated engines, VVA/VVT devices are widely employed. In the past, valve actuation systems were only used to control the intake and/or exhaust valve phasing (VVT) [21,22] or to realize different cam profiles according to the engine speed [23,24]. Most recent solutions allow to freely define the valve opening, closing and the lift (VVA) [25,26]. The versatility of the modern VVA/VVT systems involves the engine load with limited intake throttling [27,28], drastically reducing the pumping work at low/medium load. Moreover, an abatement of NO_x emissions and an improved combustion stability at idle were experimentally verified [29-31]. The combustion stability can be further enhanced if a double lift mode in each engine cycle is available, thanks to an enhanced in-cylinder turbulence [32].

High performance naturally aspirated engines usually present, especially on the intake side, some flap valves which allows to couple/decouple branches of the pipe network. In this way, the length

of the pressure wave path can be optimized and fine-tuned according to the engine rotational speed, so to maximize the cylinder filling.

Whatever is the considered engine architecture, a recent unit presents a large number of degrees of freedom. For instance, referring to a naturally aspirated engine equipped with unphased intake/exhaust VVT devices, five control parameters are available for the engine calibration:

- Air-to-fuel ratio normalized by the stoichiometric value (λ)
- Throttle valve opening
- Spark timing
- Intake valve timing
- Exhaust valve timing

To identify the optimal calibration at the test bench, each parameter has to be varied around a presumed set point. If just 5 values were explored for each parameter, a matrix of $5^5 = 3125$ experimental tests would be ideally realized in each speed-load point. However, from a practical point of view, a reduced set of optimal engine calibrations needs to be identified, once assigned the required performance targets (minimum fuel consumption, radiated noise, pollutant emissions, maximum power and torque, etc.) and constraints (catalytic converter inlet temperature, combustion stability, knock intensity, maximum in-cylinder pressure, etc.). This task is usually performed employing Design of Experiment (DoE) methodologies [31]. Nevertheless, the calibration process may require several months to be experimentally accomplished with an adequate resolution in terms of engine speed and load level, affecting development costs of a new engine.

In the light of these considerations, the possibility to carry out an engine pre-calibration through numerical models appears very desirable by engine manufacturers. In addition, coupling the model to an optimizer, a more systematic and accurate exploration of each control parameter can be realized, thus allowing to identify more precisely the optimal calibration.

As known, 3D and 1D models have been employed for several years for supporting engine development and design. 3D models are characterized of course by higher accuracy and reduced tuning efforts but, however, computing time is still incompatible to explore the whole engine operating plane. In addition, their employment is limited to the analysis of portions of the engine. 1D models, on the other hand, are capable to describe the complete engine system and to predict performance data with a minor computing effort. Accurate results can be accomplished only if proper sub-models of the in-cylinder phenomena are employed, capable to sense the variations of the engine operating conditions. The above discussion clarifies that a 1D model represents the most suitable tool to carry out a numerical engine calibration. To automatize this task, the simulation can be coupled to an optimizer, giving the possibility to identify optimal control parameters according to the selected objectives and constraints.

In the current literature, some examples of the above methodology are already available. In [33-35], for instance, an integrated 1D model/optimizer approach is followed to investigate the influence on engine performance of the fluid-dynamic behaviour of the piping system. However, a combustion description based on un-predictive Wiebe functions is considered. A more complex problem is addressed in [36], where VVT strategy, throttle position, air/fuel mixture quality ratio and spark advance are automatically modified to minimize the fuel consumption at part load. In this case, a phenomenological combustion sub-model was used. Before performing the optimization, however, a careful tuning of five parameters in the combustion model, plus an additional parameter in the heat transfer model, was carried out at each speed-load point to match the experimental burn rate. This of course implies that a large set of experimental data must be available for model tuning, thus limiting the generality and applicability of the methodology proposed in [36]. The reason for the above combustion parameters adjustment could be probably ascribed to the limited accuracy of a physical turbulence sub-model, which should provide the correct levels of turbulence intensity and length scales for combustion simulation.

The innovative contribution of this paper can be hence recognized in the application of a 1D model characterized by a single set of tuning constants allowing an accurate reproduction of the combustion process in the whole engine map. As better explained in the following, the combustion model is in fact coupled to a turbulence sub-model, preliminary tuned with reference to 3D-CFD results, under motored operation. This methodology is particularly helpful in the calibration of a VVT engine, where the turbulence levels are expected to substantially vary at part load according to the intake/exhaust valve strategies. Combustion and turbulence constants are hence selected through comparisons with few experimental data at full load and 3D results, and then employed at part load and in the optimization process, as well.

Summarizing, the aim of this work is to develop a numerical methodology able to automatically identify the optimal engine calibration of a high performance VVT naturally aspirated engine, employing refined phenomenological turbulence and combustion sub-models, not requiring any case-dependent tuning. Only in this way, the reliability of an integrated 1D model/optimizer approach can be ensured and an overall "virtual" calibration of the engine, including valve strategy, combustion phasing, turbulence level, and inert content can be accomplished.

In the following, the modelling approaches for in-cylinder phenomena will be recalled. Then, the 1D engine model will be introduced and, after a tuning phase, will be validated at full and part load, as well. Finally, the 1D engine model will be included in an automatic optimizer. This is used to identify the engine calibration minimizing the BSFC in two representative operating conditions, where the engine most frequently works along an RDE driving cycles.

Engine description and experimental tests

The considered engine is a high performance naturally aspirated V12-cylinder PFI SI unit, whose main characteristics are summarized in Table 1. Each cylinder presents a centered spark-plug and four valves. The latter are controlled by unphased VVT devices. The intake pipe network presents some flap valves which allow to couple/decouple the intake air paths. In this way, cylinder filling is optimized according to the engine speed, employing the wave dynamic effects. A muffler is installed along the exhaust line, which can be disabled by an additional flap valve.

Table 1. Main engine data.

12-cylinder VVT Naturally-Aspirated PFI Engine	
Compression ratio	11:8:1
Displaced volume, cm^3	541.54
Bore, mm	95
Stroke, mm	76.4
Connecting rod length, mm	145.8
Maximum brake power, kW	566.6 @ 8500 rpm
Maximum brake torque, Nm	720.0 @ 6750 rpm
Valve number	4 valve/cylinder

An extensive experimental campaign was carried out, investigating both the full load performance and the whole operating plane of the engine. The speed ranges from 1000 up to 8500 rpm.

The fuel is metered to realize a stoichiometric air/fuel mixture at low speeds (up to 4000 rpm). At higher speeds, the mixture is progressively enriched to favorite the vehicle drivability and to limit the exhaust temperature. The spark advance is generally set to ensure engine operation at maximum brake torque. Only at low speeds and high loads it is delayed to avoid knocking combustions. The VVT devices are controlled to maximize the torque at full load. At decreasing load, the valve timing is modified to increase their overlapping. In this way, the internal EGR is promoted, reducing the need for intake throttling.

The engine is installed at the test bench and experimentally analyzed in different operating conditions with the aim of collecting the main overall performance such as the brake power, brake torque, brake specific fuel consumption, fuel flow rate, etc. Each cylinder is equipped with a dry pressure transducer located between the intake and exhaust valves. As known, a dry sensor may be affected by uncertainty and instability with respect to a wet one, especially during the expansion phase, when the sensor undergoes relevant thermal shocks. However, in the proposed experimental activity dry sensors are selected because of their ease of installation, not requiring a coolant (water) circuit. An optical encoder is used to trigger the acquisition of the in-cylinder pressure signals. The measured signals are processed by a charge amplifier and by an analogic/digital converter. The digital output is elaborated by the indicating software for the computation of the main indicated and combustion parameters (pressure-volume diagram, IMEP, maximum in-cylinder pressure, PMEP, mass fraction burned, knock parameters, etc.) in real time. The acquisition system also provides as an output the statistical indices of the measured data. In-cylinder pressure traces are post-processed using an inverse analysis to derive the burning rate profiles and the characteristic combustion angles, namely MFB_{10}, MFB_{50} and MFB_{90}, and durations, $MFB_{0\text{-}10}$ and $MFB_{10\text{-}90}$.

For the analysis of pollutant emissions, an AVL i60 AMA 4000 system is employed. Integrated pumps draw in the measurement gas from sample points. The analysis of the gas is performed using high-end analyzers – FID for THC, CLD for NO/NOx, IRD for CO. After several correction steps, the raw values of the analyzers provide pollutant concentrations, which are transmitted to a test cell automation system.

Engine model

The tested engine is schematized and simulated in the GT-Power environment. The simulation is based on a 1D model of the unsteady flow inside the intake and exhaust pipes and a 0D model of the in-cylinder processes. The engine schematic includes cylinders, intake and exhaust pipe systems, airbox, muffler, aftertreatment and throttle valve. Only one bank is simulated, the other bank being perfectly symmetric.

A refined model of the heat transfer inside the cylinder and exhaust pipes is introduced, applying a wall temperature solver based on a finite element approach. Concerning the in-cylinder heat transfer, a Woschni-like correlation is used, while convective, radiative and conductive heat transfer modes are considered for the exhaust pipes. The combustion process is modeled using a two-zone "fractal approach" [37], where the burning rate is computed as:

$$\frac{dm_b}{dt} = \rho_u A_T S_L \quad (1)$$

ρ_u being the unburned gas density, A_T the area of the turbulent flame front and S_L the laminar flame speed. The LFS is calculated using the correlation proposed in [38].

Based on the fractal geometry theory [39,40], the ratio of the turbulent flame area, A_T, to the laminar one, A_L, namely the flame wrinkling factor, is assumed to vary according to the relation:

$$\frac{A_T}{A_L} = \left(\frac{\Gamma_{\max}}{\Gamma_{\min}} \right)^{D_3 - 2} \quad (2)$$

where $\Gamma_{\max}$ and $\Gamma_{\min}$ are the length scales of the maximum and minimum flame wrinkling, respectively, and D_3 is the fractal dimension. The flame front area A_L is computed using a CAD software package to model the intersection of a smooth spherically-shaped surface with the real 3D geometry of the combustion chamber. The estimation of $\Gamma_{\max}$, $\Gamma_{\min}$ and D_3 is based on the turbulence sub-model detailed in [41,42]. This latter is based on the solution of the balance equations of turbulent and mean flow kinetic energies, and tumble momentum. The turbulence integral length scale is reproduced as a sequence of S-shaped functions.

The knock model is based on an Auto-Ignition (AI) calculation in the unburned zone. This means that the unburned gas temperature and composition are computed also including the heat released by the AI process of the air/fuel mixture. AI calculation is carried out by a tabulated approach [43], where the AI table is derived by preliminary auto-ignition chemical kinetics simulations in a homogeneous reactor. To this aim, the kinetic scheme developed by Andrae et al. [44] is employed, including 5 elements, 185 species and 937 reactions. In the engine model, the knock event is advised as a sudden jump in the pressure and in the unburned temperature profiles.

The model also includes an estimation of the emissions namely CO, HC and NO. The model for the evaluation of CO and NO concentrations is based on a multi-zone schematization of the burned zone. A temperature stratification is supposed, where each burned parcel is assumed to compress/expand adiabatically according to the in-cylinder pressure. In each burned parcel, the CO and NO concentrations are computed starting from the equilibrium one and applying a simplified chemical kinetics. For the NO, the extended Zeldovich model is applied [45], whereas the CO variations are computed by a single-step reaction scheme [46]. Concerning the HC modeling, the literature proposes various formation mechanisms, such as the adsorption/desorption from the oil layer, wall flame quenching and crevices [47-49]. Among those mechanisms, in this work, the HC production is estimated by a very simplified methodology, where only the opposing effects of crevices HC release and thermal oxidation are considered. The unburned hydrocarbons are assumed to accumulate (be released) during the pressure rise (decrease) phase in (from) an arbitrary assigned constant volume [47]. It schematizes the crevices in the combustion chamber, where the flame front extinguishes. In this volume, the temperature is considered the same as the wall one, while the pressure is supposed equal to the cylinder one. The mass (or moles) released in each time step is computed by the universal gas law, assuming a gas composition equal to the unburned mixture. The unburned hydrocarbons emanated from the crevices are assumed to burn with an oxidation rate determined by the empirical correlation proposed in [48]. This depends on the HC and molecular oxygen concentrations and on the temperature. The oxidation temperature is computed as a

weighted average between the in-cylinder mean gas temperature and the wall temperature [49].

Engine Model Tuning

The first stage of the model tuning is the identification of the constants for the turbulence sub-model, according to a hierarchical 1D/3D methodology as deeply discussed in previous works by the present authors [41, 42]. The constants are adjusted by fitting the results of an in-cylinder 3D CFD simulation for a speed of 6750 rpm under motored conditions. Time-varying boundary conditions at the intake and exhaust ports are derived from 1D simulations. The adopted model has been widely validated for different engines under various operating conditions and valve strategies [42]. The results of the turbulence model are compared with the 3D outcomes in Figure 1, during the intake, compression and expansion strokes (the y-axis scale is hidden because of confidentiality reasons). The agreement is quite satisfactory, the 1D model being capable to describe satisfactorily the level and the quick turbulence decay across the TDC. It is worth to underline that an accurate turbulence prediction during this phase is a mandatory prerequisite for a reliable combustion description.

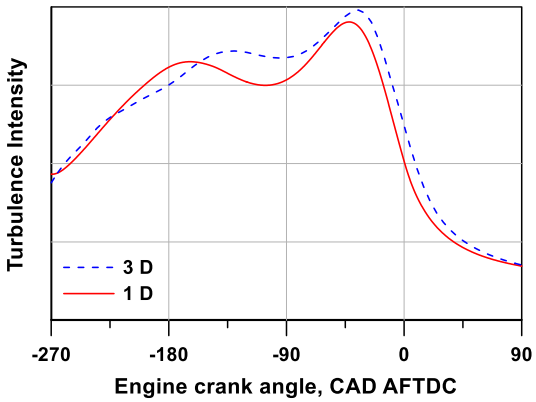

Figure 1. 1D/3D comparison of turbulence intensity at 6250 rpm under motored operations.

Concerning the combustion model, it is tuned at full load to reproduce the experimental burning rates and in-cylinder pressure cycles. The combustion model includes three tuning constants [37], which selectively affect the different stages of the combustion. The first constant, named c_{trans}, controls the transition between an initially laminar flame and a fully-turbulent combustion by progressively increasing fractal dimension D_3 in Eq. (2). D_3 changes over time as a function of a characteristic time scale weighted by c_{trans}. The duration of the laminar-to-turbulent transition lengthens as c_{trans} increases. During the transition, D_3 changes from a value representative of laminar combustion (2.0) to a value typical of fully developed flames (up to 2.35). This latter depends on the laminar flame speed and turbulence intensity, and it is estimated using the empirical correlation proposed in [50]. The second constant, c_{wrk}, is a multiplier of maximum wrinkling scale Γ_{max}, and its increase causes an overall speed-up of the combustion process. The third constant, x_{wc}, controls the impact of the wall-combustion stage. The burning rate slowdown, typical of this stage, is mimicked by a progressive transition to a laminar flame. The weight of the wall-combustion is increased according to the ratio between the surface area of the combustion chamber wetted by the flame and the total surface area of the chamber. A higher value of x_{wc} results in a faster turbulent-to-laminar transition and hence in a longer combustion tail. The combustion constants have been identified considering only full load operations over the whole variation range of the engine speed. More details about the role of these constants in the combustion model and the tuning procedure are reported in [37].

Model Validation at Full Load

For the full load analysis, the experimentally actuated λ and valve timing are imposed as input data in the simulations. The positions of the intake/exhaust flap valves are assigned according to the experiments, as well. The throttle valve is assumed fully opened. The spark advance is not directly imposed, but it is identified by an automatic controller implemented in the combustion model which targets the measured MFB_{50}. 33 operating points (from 1000 up to 8500 rpm,) are simulated. As a first verification of the model consistency, in Figure 2-Figure 4 the numerical/experimental comparison of the BMEP, BSFC and in-cylinder peak pressure are shown. Due to confidentiality reasons, the scales of the plots are hidden. The figures also show the RMSD for each considered performance parameter and the error bands of ± 5%. It can be observed that most of the points lie in the error bands, denoting the good accuracy in the engine geometry schematization and in the combustion/turbulence modeling. Some systematic underestimations concern the BSFC predictions, which are probably due to the inaccuracies in heat transfer modelling. The errors for most points are below 5% for this parameter. The accurate schematization of the engine piping is further proved by the experimental/numerical comparisons of the intake and exhaust traces at different engine speeds, shown in Figure 7. The picture underlines that the pressure fluctuations are very well captured by the model, both in terms of shape and pulse amplitude, for all the considered speeds.

A first insight in the combustion model reliability is given by the numerical/experimental assessment between the characteristic durations of the early combustion stage $MFB_{0\text{-}10}$ and of its core $MFB_{10\text{-}90}$, shown in Figure 5 and Figure 6, respectively. The figures also show error bands of ±2 CADs and ±5 CADs. The points present a reduced scattering around the zero-error line, with a RMSD of about 2 and 2.5 CADs for the $MFB_{0\text{-}10}$ and $MFB_{10\text{-}90}$, respectively. For the latter duration, a certain systematic model overestimation occurs, which is probably due to an inaccurate prediction of the heat losses during the last stage of the combustion process. To further prove the combustion model accuracy, the experimental/numerical comparisons of the in-cylinder pressure cycles and the related burning rates are depicted in Figure 8. In all the operating points, the agreement is very good, especially in terms of burning rate profile. As a final remark, the simulations highlight that a certain knock intensity appears in the operating points at full load with an engine speed below 4000 rpm. This is coherent with the need emerged in the experimental tests, where the MFB_{50} is delayed at those speeds to control the knock.

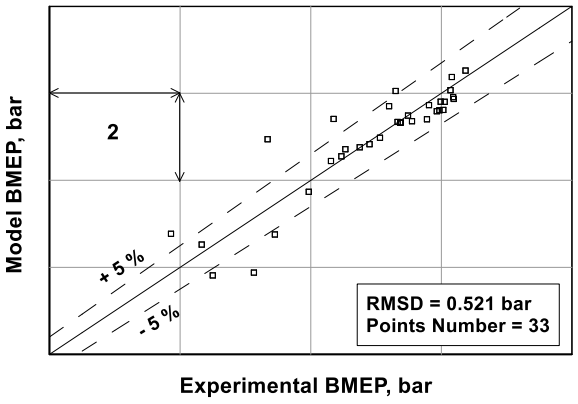

Figure 2. Experimental vs. numerical BMEP at full load.

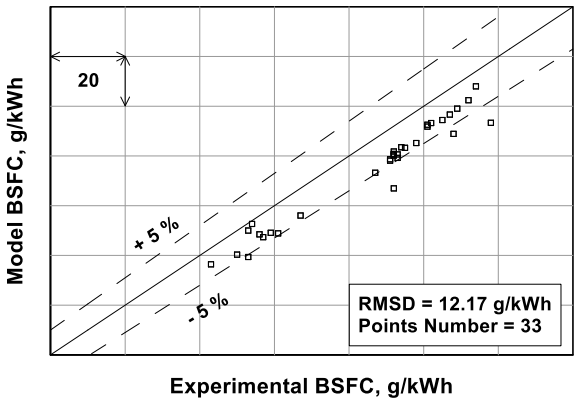

Figure 3. Experimental vs. numerical BSFC at full load.

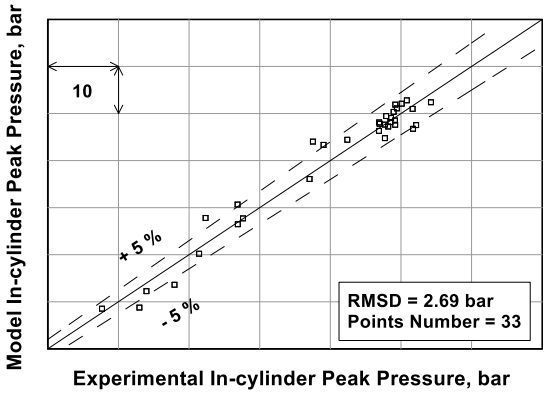

Figure 4. Experimental vs. numerical in-cylinder peak pressure at full load.

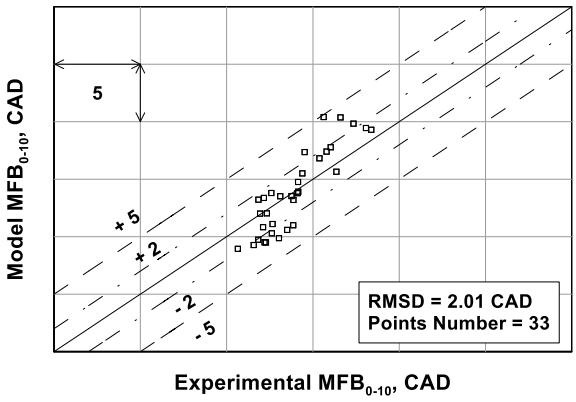

Figure 5. Experimental vs. numerical MFB_{0-10} at full load.

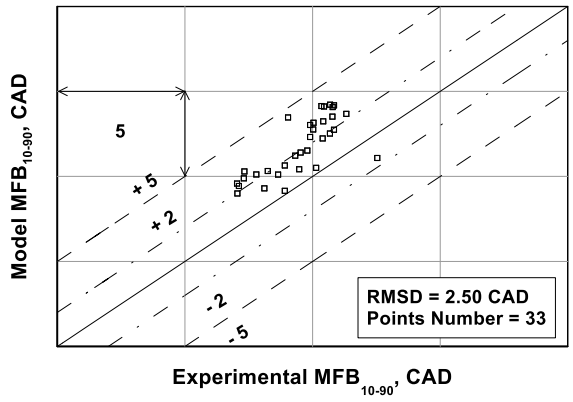

Figure 6. Experimental vs. numerical MFB_{10-90} at full load.

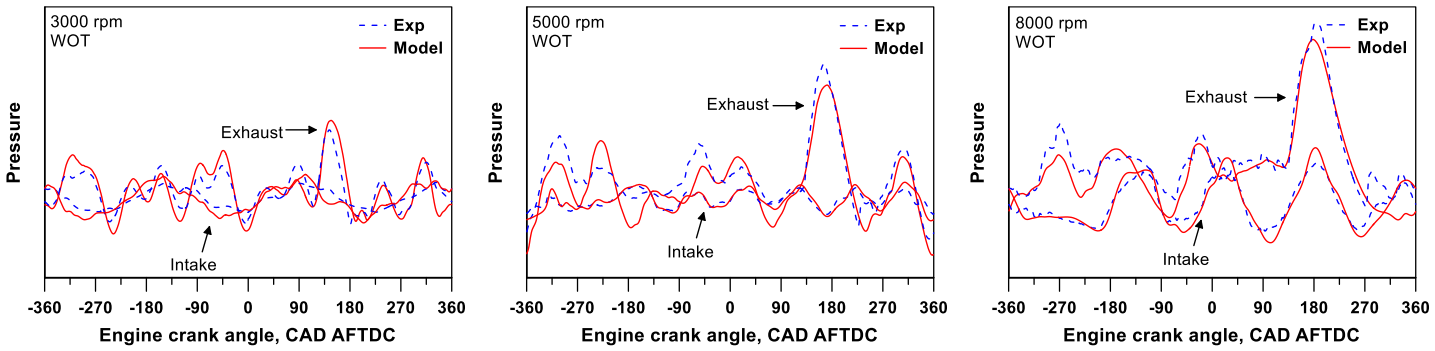

Figure 7. Experimental/numerical assessment of the intake and exhaust pressure traces at 3000, 5000 and 8000 rpm WOT.

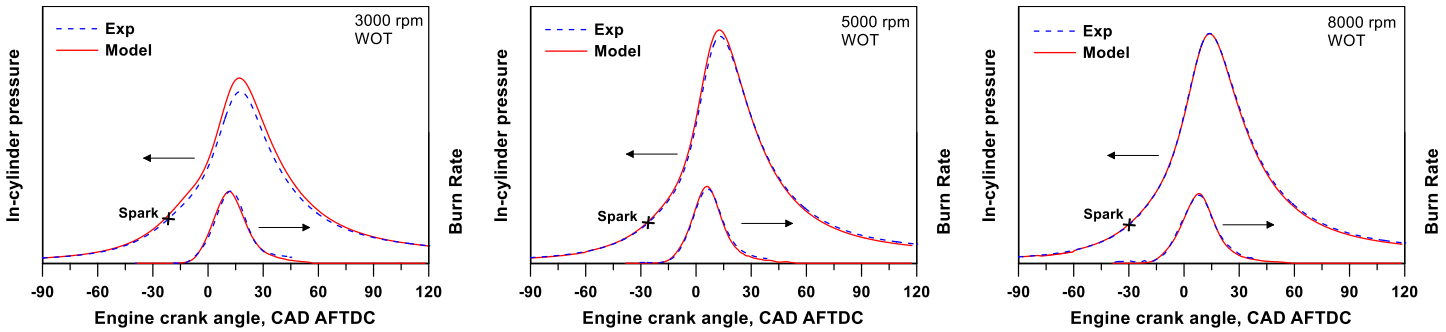

Figure 8. Experimental/numerical assessment of the in-cylinder pressure traces at 3000, 5000 and 8000 rpm WOT.

Model Validation at Part Load

The model consistency is verified over the whole engine operating plane, based on the experimental data collected under part load conditions. To this aim, the tuning of turbulence / combustion / heat transfer model is not modified compared to the full load analysis. The simulation inputs are the same as the full load setup, namely, the intake/exhaust valve timing, the flap position, the air/fuel mixture quality and the MFB_{50}. The only difference regards the throttle valve opening, which is modulated by an automatic controller targeting the measured BMEP level. The simulation reliability is here verified by comparing the experimental/numerical maps of BSFC, combustion duration $MFB_{10\text{-}90}$, exhaust temperature and raw concentrations of CO, HC and NO (upstream the catalytic converter).

For reasons of confidentiality, the BMEP scale is normalized by its maximum value, along with the iso-contours of internal EGR percentage, exhaust temperature and pollutant emissions. Instead, BSFC, λ, and $MFB_{10\text{-}90}$ are normalized by their minimum levels over the whole engine plane. Excepting for the pollutant emission plots, for all the other comparisons the same level and grayscale are chosen for the measured and calculated data, so to favorite the figures readability and comparability.

Starting from the experimental/numerical BSFC comparison of Figure 9, it can be observed that the model is able to reproduce the measured data with an adequate accuracy. It is able to correctly detect the level and the speed-BMEP range of minimum fuel consumption. In addition, it shows the capability to perceive the BSFC worsening at increasing speed, which is mainly due to the air/fuel mixture enrichment, and at reducing load, which is affected by the intake throttling. The computed and experimental contours of combustion duration $MFB_{10\text{-}90}$ in Figure 10 present similar shapes. As well as the full load simulations, the model slightly overestimates this parameter compared to the experimental outcomes, excepting in the region of very low load. Figure 10 highlights a combustion lengthening for speeds below 4000 rpm, which is due to the activation of the muffler along the exhaust line. This causes an increased backpressure and a higher level of residual gas in the cylinder, affecting the combustion speed. The model shows to perceive quite well this phenomenology, as demonstrated by the experimental/numerical comparison in Figure 10. The residual amount estimated by the model is plotted in Figure 11. The latter underlines that the residual content is quite low for this engine over the whole operating plane, and even at low load. As a further demonstration of the model consistency, the experimental and numerical iso-lines of exhaust temperature are plotted in Figure 12. The maps are similar in terms of both shape and level. The expected temperature increase at rising engine speed is partially compensated by the air/fuel enrichment, highlighted in Figure 11. The maximum temperature occurs at high speed and low load, which can be considered as the upper limit allowable for the aftertreatment device.

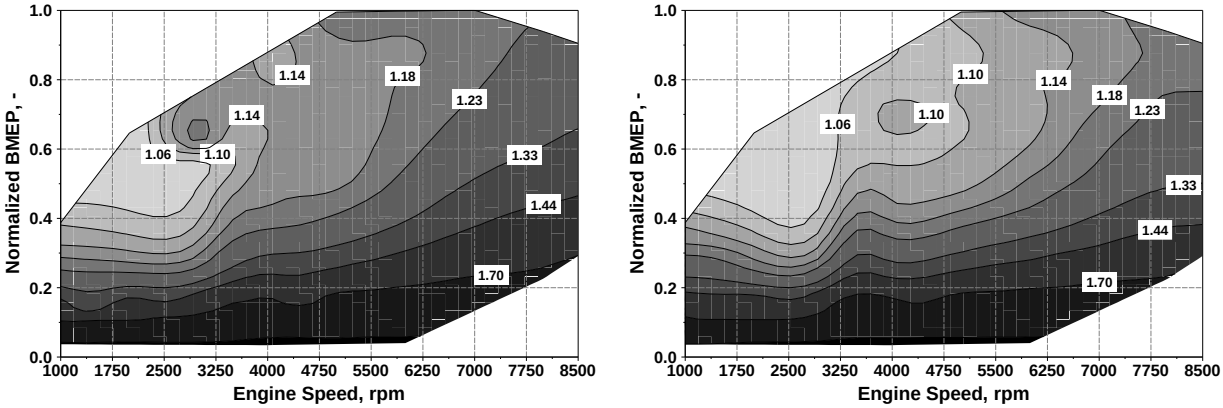

Figure 9. Experimental (left) and numerical (right) BSFC maps (normalized by the minimum experimental level).

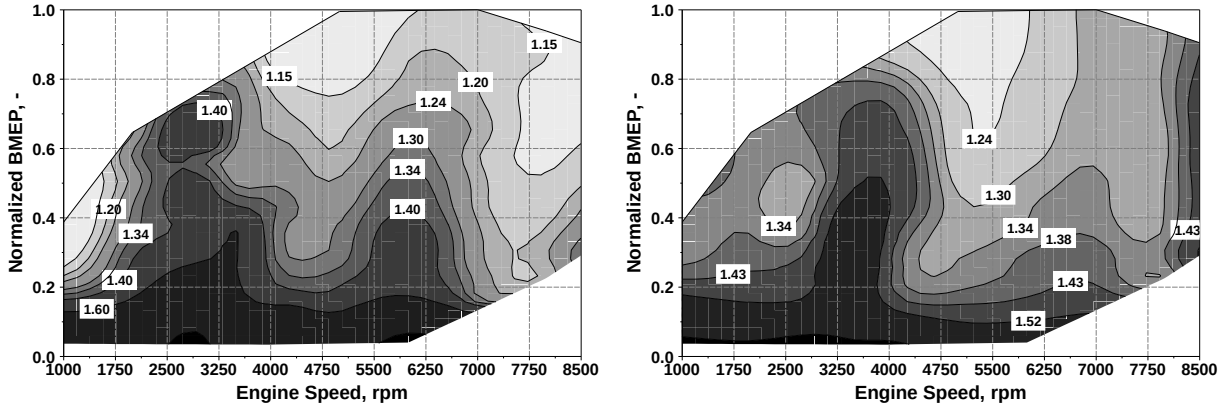

Figure 10. Experimental (left) and numerical (right) $MFB_{10\text{-}90}$ maps (normalized by the minimum experimental level).

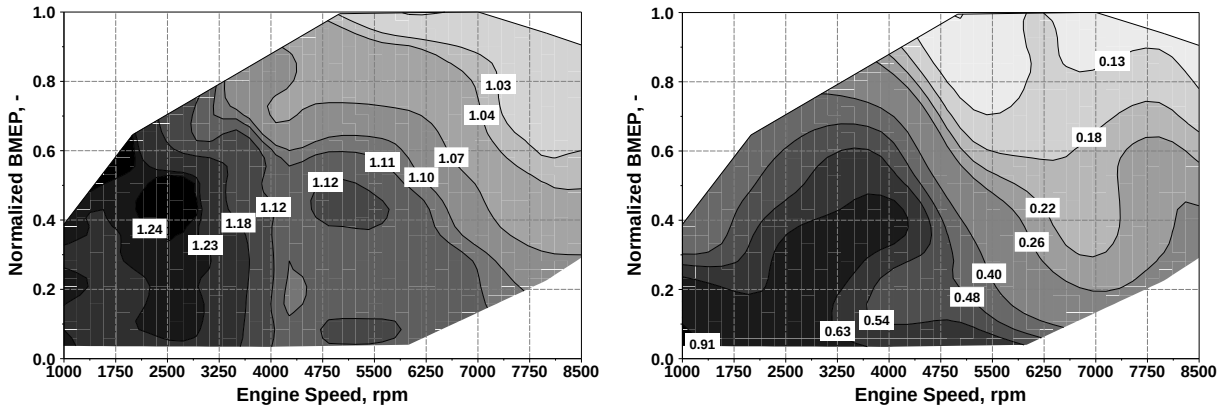

Figure 11. λ map (normalized by the minimum level) (left) and numerically estimated internal EGR map (normalized by the maximum level) (right).

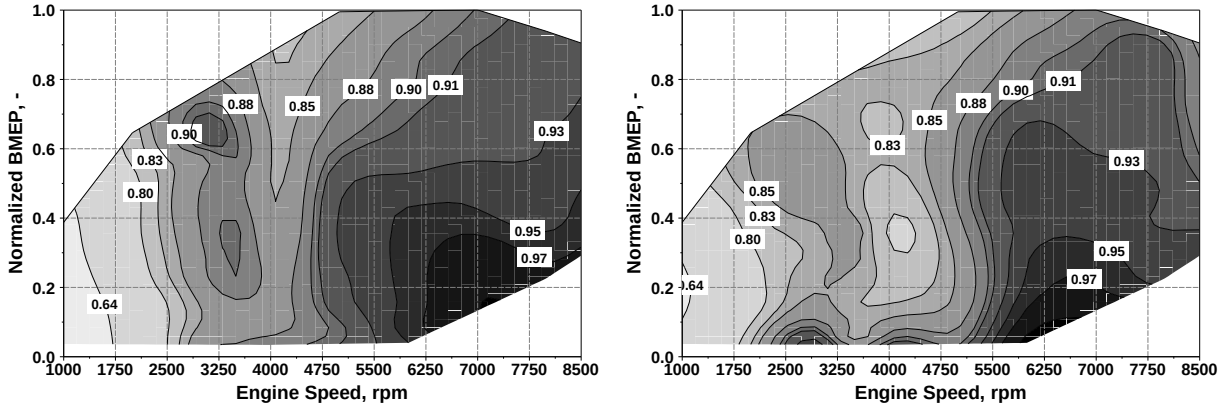

Figure 12. Experimental (left) and numerical (right) exhaust temperature maps (normalized by the maximum experimental level).

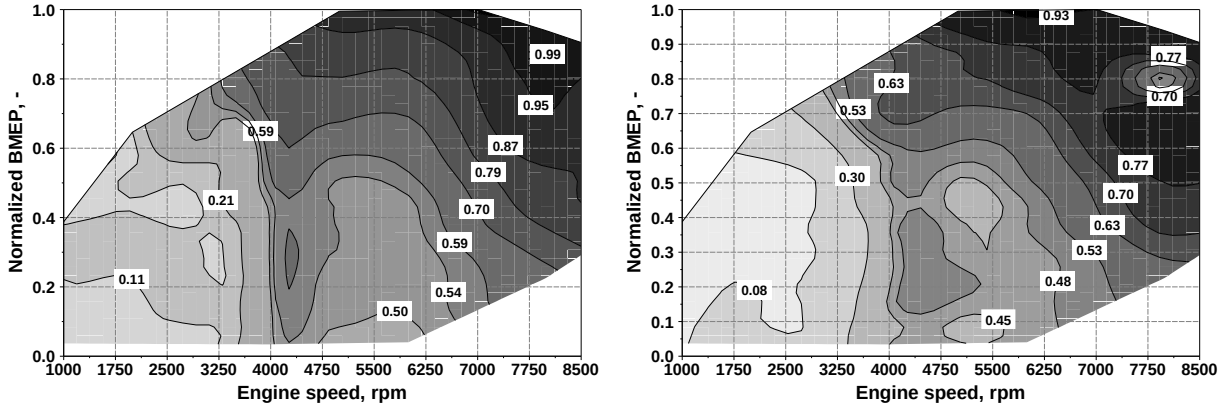

Figure 13. Experimental (left) and numerical (right) CO concentration maps (normalized by the maximum experimental level).

The model also provides an estimation of the raw emissions of CO, HC and NO. These are assessed with the related measured data in Figure 13, Figure 14 and Figure 15, respectively. The iso-contour shapes of the emission maps resemble the corresponding experimental counterparts, but the predicted levels are in most cases quite different. Starting from the CO concentration prediction, the model demonstrates to sense effects of the air/fuel enrichment, which results in a higher CO production. However, numerical estimations are about 19% lower than the measured concentration on average. The HC numerical estimation is less accurate, especially at very low load. This is probably due to an overestimation of the post-oxidation effect under such operating conditions. The model detects the reduced HC production around the 3500 rpm and higher levels at high speed and medium loads. On the contrary, the simulation is not able to perceive the increase of HC emissions at the lowest speeds and in the speed range 4000-5500 rpm close to the full load operations. Despite the highlighted errors, the model predictions can be considered adequately accurate (with a percent error of about 31% on average) in the light of the adopted very simplified approach, which does not consider some HC formation mechanisms. Moving to the NO model response, the related experimental/numerical maps in Figure 15 present very similar shapes of the iso-NO curves. Maximum NO concentrations, in accordance with the measurements, are estimated in the region where the λ values are close to the

stoichiometric levels, which simultaneously determine higher in-cylinder temperatures and lack of molecular oxygen in the burned gas. However, the simulation gives on average a NO prediction lower than the experimental counterpart, with an underestimation of about 58% on average. This is probably due to a global underestimation of the in-cylinder temperatures or to an inaccurate description of temperature stratification.

The proposed results about the pollutant emissions put into evidence that the numerical approach is not enough advanced to quantitatively predict the experimental data, although the variations with the engine operating parameters (speed, load, λ) are captured. For this reason, the model will be employed in the following to draw the variation trend of the pollutant emissions changing the engine calibration, rather than to predict their absolute levels.

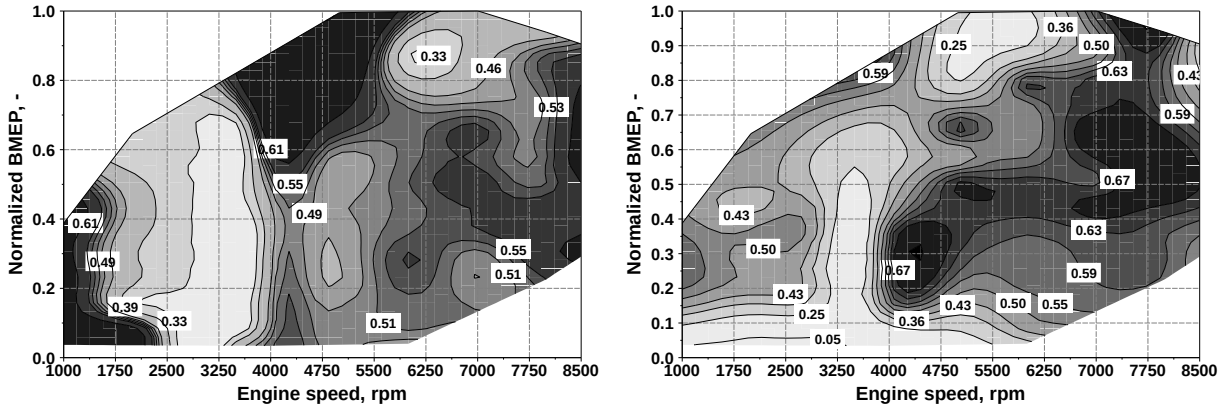

Figure 14. Experimental (left) and numerical (right) HC concentration maps (normalized by the maximum experimental level).

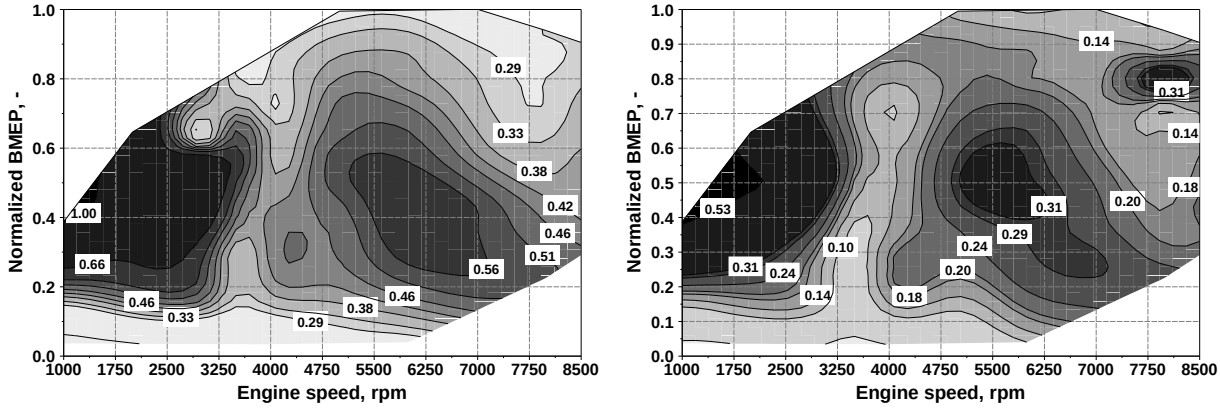

Figure 15. Experimental (left) and numerical (right) NO concentration maps (normalized by the maximum experimental level).

Optimization Procedure Description

Figure 16 illustrates the logical schematic of the optimization procedure. As first step the control parameters are defined, namely the intake valve opening angle and exhaust valve closure one (IVO and EVC, respectively) and the combustion phasing MFB_{50}. For each step of the procedure, these parameters are passed to the 1D engine model and a single analysis is performed at a predefined engine speed and BMEP. Likewise to the part load analyses, the load target is matched in the simulation by modulating the throttle valve opening. At the end of each 1D model calculation, the computed BSFC is extracted and passed back to the optimizer for the next iteration, until optimal values are identified. Other parameters are extracted, which characterize the engine calibration and performance, namely $MFB_{0\text{-}10}$, $MFB_{10\text{-}90}$, PMEP, pollutant emissions and the in-cylinder residual fraction. The configurations leading to the exceeding of some imposed constraints are considered as "unfeasible" and discarded by the optimization process. In particular, the maximum allowed level of x_r is 20%, with the aim to limit the cycle-by-cycle variations potentially occurring on the real engine. Such limitation arises from the engine manufacturer know-how.

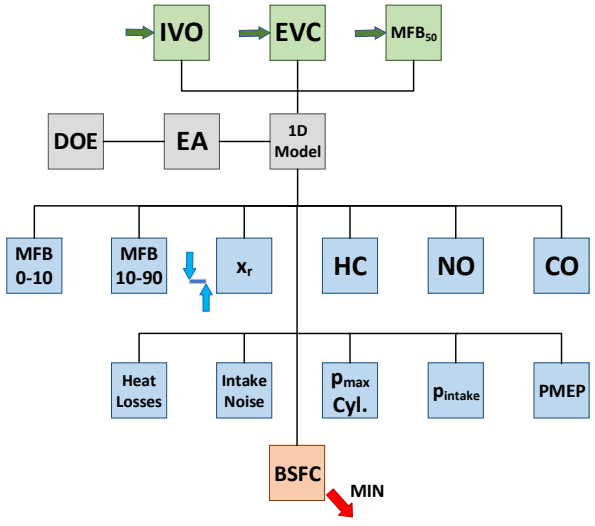

Figure 16. Schematic of the optimization procedure.

Before the activation of the optimization process, a preliminary exploration of the engine response to "first attempt" calibrations are carried by a DoE methodology. In this phase, as a first step, the experimentally identified calibration is numerically tested. Subsequently, the optimization begins. It is based on a genetic algorithm, belonging to the category of Evolutionary Algorithms (EAs). As known, EAs mimic the natural evolutionary process by introducing the principles of "survival of the fittest" and genetics theory. Typically, they are characterized by higher robustness in identifying the global minimum compared to the gradient methods, although a higher number of evaluations is required to get the optimum [51]. An extensive discussion on the genetic EAs and suggestions on customized forms for a variety of applications can be found in [52].

Optimization Results Discussion

The above described optimization procedure is applied to the conditions where the engine most frequently works along an RDE driving cycles. To this aim, a vehicle model is setup for investigating RDE worst case scenario for a defined engine-vehicle combination. The worst-case cycle is defined by the combination of all the relevant events which lead to the highest consumption/emissions. The identified engine points most used during this RDE cycle are 3000@2, 3000@6, 4000@3, 5000@3, 5000@12, where the above notation indicates the rpm/BMEP (bar) couple.

The discussion of this section refers to two representative points, 3000@2 and 5000@12, characterized by very different loads. Results leading to analogous comments are found for the other operating conditions and they will not be mentioned here for sake of brevity. In all those points, preliminary simulations highlighted that the engine operates under knock-free conditions. For this reason, no limitation of the spark advance is applied to control the knock intensity. The analyses also showed that the exhaust temperature at the TWC inlet is not a critic issue in the chosen points.

In all the investigated operating conditions, hundreds of simulations are carried out by the optimizer until the minimum BSFC is found. At the end of the optimization process, the best configuration is selected and compared with the experimentally identified calibration. Starting the discussion from the point 3000@2, the comparisons between the two configurations are shown in Figure 17-Figure 19 under the form of bar charts. In those figures, the bar charts related to the base configuration represent the reference values, stated conventionally equal to 1. The optimal configuration results are compared to the base ones in terms of fraction. Such a normalization is once more for reasons of confidentiality. Figure 17 shows the assessments of the considered calibration parameters (EVC, IVO and MFB_{50}) and the corresponding BSFC. It can be observed that this last reduces of about 4.7 % thanks to the identified optimal engine calibration. The main driver to get this result is an optimized combustion phasing and a delayed timing of both valves, leading to a reduced pumping work (Figure 18). This is also favoured by a certain increase of the valve overlapping.

The identified engine configuration causes some drawbacks, such as slightly higher heat losses, a much higher gas-dynamic noise radiated by the intake mouth and a greater residual percentage (Figure 18). It also reflects on the combustion process, in a way more pronounced on the its early stage, $MFB_{0\text{-}10}$, rather than on its core, $MFB_{10\text{-}90}$. The more advanced combustion phasing (lesser in-cylinder pressure and temperature at the spark), together with the higher residual content, lead to slower combustion speeds, especially at the combustion beginning. Another critical issue of the optimal engine calibration, not straightforwardly detectable by the adopted numerical approach, is the onset of combustion instabilities and inacceptable cycle-by-cycle variations. These last may arise on a real engine under such a condition.

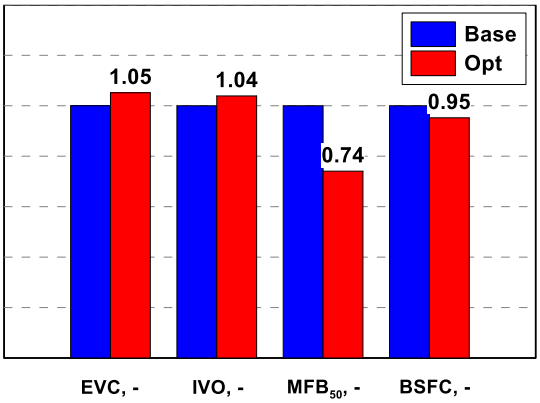

Figure 17. Base and optimized calibration comparison at 3000@2: EVC, IVO, MFB_{50} and BSFC.

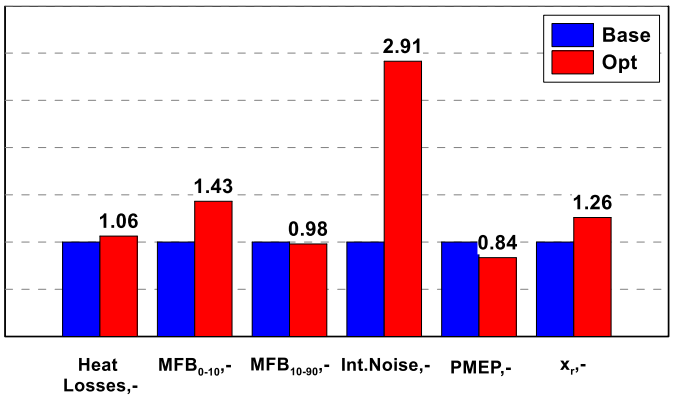

Figure 18. Base and optimized calibration comparison at 3000@2: heat losses, $MFB_{0\text{-}10}$, $MFB_{10\text{-}90}$, intake gas-dynamic noise, PMEP and residual gas percentage (values normalized by the level of the base calibration).

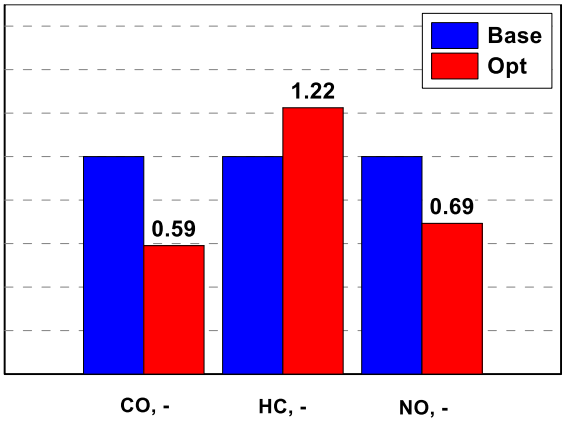

Figure 19. Base and optimized calibration comparison at 3000@2: concentrations of CO, HC and NO (values normalized by the level of the base calibration).

Based on the above discussion, the identified optimal calibration, although resulting a substantially much better fuel consumption, requires an experimental verification to be confirmed or properly modified. This calibration also reflects on the pollutants production, as shown in Figure 19. The optimal configuration leads to lower

temperature in the burned zone, which in turn results in a lesser production of CO and NO, but this also causes a less effective post-oxidation of the HC during the expansion stoke.

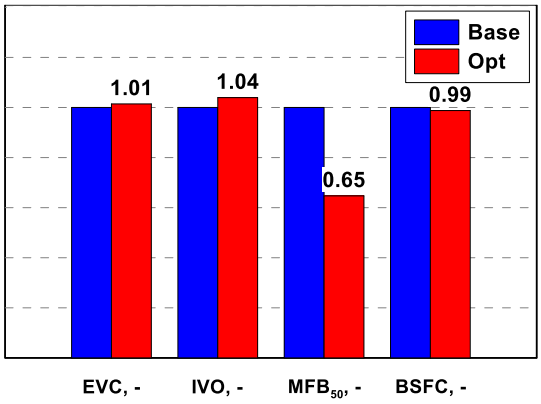

Figure 20. Base and optimized calibration comparison at 5000@12: EVC, IVO, MFB_{50} and BSFC.

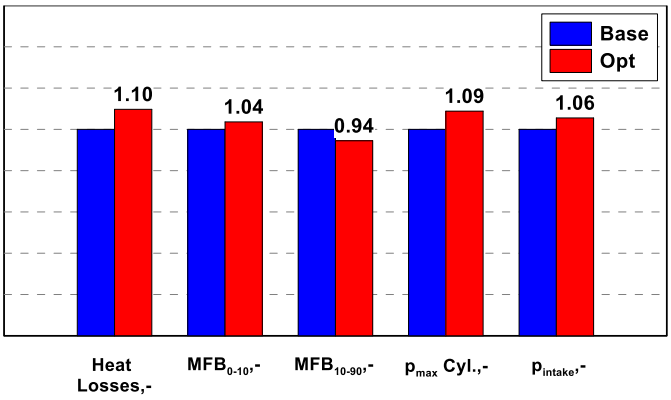

Figure 21. Base and optimized calibration comparison at 5000@12: heat losses, $MFB_{0\text{-}10}$, $MFB_{10\text{-}90}$, intake gas-dynamic noise, PMEP and residual gas percentage (values normalized by the level of the base calibration).

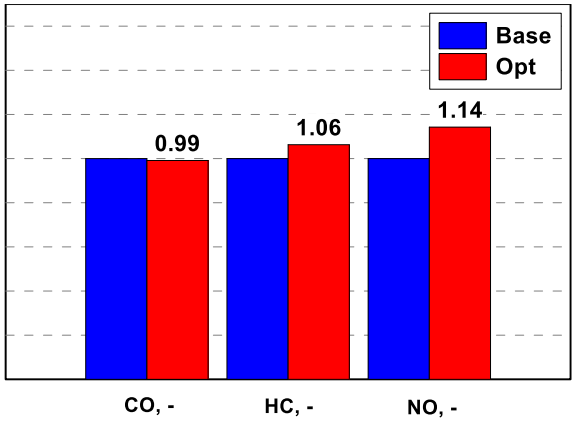

Figure 22. Base and optimized calibration comparison at 5000@12: concentrations of CO, HC and NO (values normalized by the level of the base calibration).

In the second considered operating condition, 5000@12, the optimization process gives as optimal calibration a configuration close to the experimental one, as shown in the comparisons of Figure 20-Figure 22. Also in this operating point, the optimal solution involves a delay of both intake and exhaust timing and a reduction of the valves overlapping. This contributes to improve the cylinder filling, as highlighted by the increase in the intake pressure. The optimizer also indicates to advance the MFB_{50} to improve the thermodynamic efficiency. The numerically identified engine calibration however leads to a reduced BSFC improvement (about 1.1%). The combustion phasing modification causes some drawbacks, such as higher heat losses and in-cylinder pressure peaks (Figure 21).The optimal calibration marginally affects the combustion process in terms of characteristic durations $MFB_{0\text{-}10}$ and $MFB_{10\text{-}90}$. A reduced effect is exerted on the pollutant emissions, as shown in Figure 22.

The proposed calibration methodology can be easily applied to different operating conditions and/or extended to the whole engine plane, adding to the optimization decision parameters the engine speed and the throttle valve position. In this way, a “pre-calibration” of the engine can be identified, which can help to support and drive the experimental activity.

Conclusions

The paper describes a numerical methodology aiming to calibrate a naturally aspirated spark ignition engine equipped with VVT on both intake and exhaust sides. The engine model is developed in GT-Power environment and is integrated with “user routines” for turbulence, combustion and pollutants production description. Concerning turbulence model tuning, numerical 3D CFD outcomes are utilized, whereas experimental data at full load operation are employed to tune the combustion model. The 1D model is then validated at part load, without introducing any modification in the tuning constants, and still denoting a satisfactory agreement with the experimental findings.

The model is then coupled to an optimizer with the aim of searching the calibration strategy that minimizes the fuel consumption in two operating conditions, where the engine most frequently works along an RDE driving cycles, namely 3000@2 and 5000@12. The optimized parameters are the valves timing and the combustion phasing. For the first point, the identified optimal engine calibration allows to improve the BSFC of about 4.7 % compared to the experimentally-chosen configuration, mainly thanks to a smaller pumping work. Some drawbacks are highlighted, especially in terms of combustion lengthening and gas-dynamic noise. In the second investigated point, the numerically-identified optimal calibration is close to the experimental one, leading to a fuel consumption reduction of about 1.1 %. In this case, the configuration which maximize the cylinder filling is found as optimal.

The proposed methodology proved to be a valuable tool to realize a “virtual” engine calibration being capable to perceive on physical basis the effects of engine control parameters. If applied in an industrial environment, and utilizing more advanced optimization strategies, it will hence contribute to drastically reduce time and costs related to experimental activities at the test bench.

Contact information

References

1. European Environment Agency, "Annual European Union greenhouse gas inventory 1990–2012 and inventory report 2014," Report No.: 9/2014", 2014.
2. Wirth, M., Schulte, H., "Downsizing and Stratified Operation – An Attractive Combination Based on a Spray-guided Combustion System," presented at Intl. Conference on Automotive Technologies, Istanbul, 2006.
3. Police, G., Diana, S., Giglio, V., Iorio, B., Rispoli, N., "Downsizing by SI-Engines by Turbo-Charging," presented at 8th Biennal ASME Conference on Engineering Systems Design and Analysis, Italy, July 4, 2006.
4. Boretti, A., Scalzo, J., "Exploring the Advantages of Variable Compression Ratio in Internal Combustion Engines by Using Engine Performance Simulations," SAE Technical Paper 2011-01-0364, 2011, doi: 10.4271/2011-01-0364.
5. Shelby, M.H., Leone, T.G., Byrd, K.D., Wong, F.K., "Fuel Economy Potential of Variable Compression Ratio for Light Duty Vehicles," *SAE Int. J. Engines*10(3):817-831, 2017, doi: 10.4271/2017-01-0639.
6. Tomazic D., Kleeberg, H., Bowyer, S., Dohmen, J., Wittek, K, Haake, B., "Two-Stage Variable Compression Ratio (VCR) System to Increase Efficiency in Gasoline Powertrains," DEER Conference 2012, Dearborn, Oct. 16, 2012, doi: 10.4271/2013-01-0288.
7. Wittek, K., Tiemann, C., Pischinger, S., "Two-Stage Variable Compression Ratio with Eccentric Piston Pin and Exploitation of Crank Train Forces," *SAE Int. J. Engines* 2(1):1304-1313, 2009, doi:10.4271/2009-01-1457.
8. Ferrey, P., Miehe, Y., Constensou, C., Collee, V., "Potential of a Variable Compression Ratio Gasoline SI Engine with Very High Expansion Ratio and Variable Valve Actuation," *SAE Int. J. Engines* 7(1):468-487, 2014, doi:10.4271/2014-01-1201.
9. Francqueville, L., Michel, J., "On the Effects of EGR on Spark-Ignited Gasoline Combustion at High Load," *SAE Int. J. Engines* 7(4):1808-1823, 2014, doi:10.4271/2014-01-2628.
10. Cairns, A., Blaxill, H., Irlam, G., "Exhaust Gas Recirculation for Improved Part and Full Load Fuel Economy in a Turbocharged Gasoline Engine," SAE Technical Paper 2006-01-0047, 2006, doi:10.4271/2006-01-0047.
11. Potteau, S., Lutz, P., Leroux, S., Moroz, S. et al., "Cooled EGR for a Turbo SI Engine to Reduce Knocking and Fuel Consumption," SAE Technical Paper 2007-01-3978, 2007, doi:10.4271/2007-01- 3978.
12. Alger, T., Chauvet, T., Dimitrova, Z., "Synergies between High EGR Operation and GDI Systems," *SAE Int. J. Engines* 1(1):101- 114, 2008, doi:10.4271/2008-01-0134.
13. Fontana, G., Galloni, E., "Experimental analysis of a spark-ignition engine using exhaust gas recycle at WOT operation," *Applied Energy* 87(7):2187-2193, 2010, doi: 10.1016/j.apenergy.2009.11.022.
14. Grandin, B., Angström, H., "Replacing Fuel Enrichment in a Turbo Charged SI Engine: Lean Burn or Cooled EGR," SAE Technical Paper 1999-01-3505, 1999, doi: 10.4271/1999-01-3505.
15. Hoppe, F., Thewes, M., Baumgarten, H. and Dohmen, J., "Water injection for gasoline engines: Potentials, challenges, and solutions," *International J of Engine Research* 17(1):86-96, 2016, doi: 10.1177/1468087415599867.
16. Soyelmez, M., Ozcan, H., "Water Injection Effects on the Performance of Four-Cylinder, LPG Fuelled SI Engine," *Open Access Scientific Reports* 2(1), 2013, doi: 10.4172/scientificreports.591.
17. Busuttil, D., Farrugia, M., "Experimental Investigation on the Effect of Injecting Water to the Air to Fuel Mixture in a Spark Ignition Engine," *MM (Modern Machinery) Science Journal* 1:585-590, 2015, doi: 10.17973/MMSJ.2015_03_201510.
18. Sens, M., Binder, E., "Pre-Chamber Ignition as a Key Technology for Future Powertrain Fleets," *MTZ Worldwide* 80(2): 44–51, 2019, doi: 10.1007/s38313-018-0150-1.
19. Roethlisberger, R., Favrat, D., "Comparison between direct and indirect (prechamber) spark ignition in the case of a cogeneration natural gas engine, part I: engine geometrical parameters," *Applied Thermal Engineering* 22(11), 1217-1229, 2002, doi: 10.1016/S1359-4311(02)00040-6.
20. Mueller, C., Morcinkowski, B., Schernus, C., Habermann, K., Uhlmann, T., "Development of a pre-chamber for spark ignition engines in vehicle applications," 4th International Conference on Ignition Systems for Gasoline Engines, Dec. 2018, doi: 10.5445/IR/1000088588.
21. Moriya Y., Watanabe A., Uda H., Kawamura H., Yoshioka M., Adachi M., "A Newly Developed Intelligent Variable Valve Timing System – Continuously Controlled Cam Phasing as Applied to a New 3 Liter Inline 6 Engine," SAE Technical Paper 960579, 1996, doi: 10.4271/960579.
22. Maekawa K., Ohsawa N., Akasaka A., "Development of a Valve Timing Control System," SAE Technical Paper 890680, 1989, doi: 10.4271/890680.
23. Sellnau, M., Kunz, T., Sinnamon, J., Burkhard, J., "2-step Variable Valve Actuation: System Optimization and Integration on an SI Engine," SAE Technical paper 2006-01-0040, 2006, doi: 10.4271/2006-01-0040.
24. Hatano, K., Lida, K., Higashi, H., Murata, S., "Development of a New Multi-Mode Variable Valve Timing Engine," SAE Technical Paper 930878, 1993, doi: 10.4271/930878.
25. Theobald, M., Lequesne, B., Henry, R., "Control of Engine Load via Electromagnetic Valve Actuators," SAE Technical Paper 940816, 1994, doi: 10.4271/940816.
26. Luisi, S., Doria, V., Stroppiana, A., Millo, F. et al., "Experimental Investigation on Early and Late Intake Valve Closures for Knock Mitigation through Miller Cycle in a Downsized Turbocharged Engine," SAE Technical Paper 2015-01-0760, 2015, doi: 10.4271/2015-01-0760.
27. Tuttle, J., "Controlling Engine Load by Means of Late Intake-Valve Closing," SAE Technical Paper 800794, 1980, doi: 10.4271/800794.
28. Urata, Y., Umiyama, H., Shimizu, K., Fujiyoshi, Y., Sono, H., Fukuo, K., "A Study of Vehicle Equipped with Non-Throttling S. I. Engine with Early Intake Valve Closing Mechanism," SAE Technical Paper 930820, 1993, doi: 10.4271/930820.
29. Lee, J., Lee, C., Nitkiewicz, J., "The Application of a Lost Motion VVT System to a DOHC SI Engine," SAE Technical Paper 950816, 1995, doi: 10.4271/950816.
30. Leone, T., Christenson, E., and Stein, R., "Comparison of Variable Camshaft Timing Strategies at Part Load," SAE Technical Paper 960584, 1996, doi: 10.4271/960584.
31. Roepke, K., Fischer, M., "Efficient Layout and Calibration of Variable Valve Trains," SAE Technical Paper 2001-01-0668, 2001, doi: 10.4271/2001-01-0668.
32. Bozza, F., De Bellis, V., Gimelli, A., and Muccillo, M., "Strategies for Improving Fuel Consumption at Part-Load in a Downsized Turbocharged SI Engine: a Comparative Study," *SAE Int. J. Engines* 7(1):60-71, 2014, doi:10.4271/2014-01-1064.
33. Mohiuddin, A., Rahman, A., Shin, Y. "Application of Multi-Objective Genetic Algorithm (MOGA) for Design Optimization of Valve Timing at Various Engine Speeds," *Advanced Materials Research*, 264-265:1719-1724, 2011, doi: 10.4028/www.scientific.net/AMR.264-265.1719.
34. Maiani, F., Sisi, A., Leardini, W., "Multi-Objective Optimization of the Timing System on a Small 2-Wheeler

Engine (SOHC): Methodology and Case Study," SAE Technical paper 2014-32-0055, 2014, doi: 10.4271/2014-32-0055.
35. D'Errico, G., Cerri, T., Pertusi, G., "Multi-objective optimization of internal combustion engine by means of 1D fluid-dynamic models," *Applied Energy* 88(3): 767-777, 2011, doi: 10.1016/j.apenergy.2010.09.001.
36. Zhao, J., Xu, M., "Fuel economy optimization of an Atkinson cycle engine using genetic algorithm," *Applied Energy* 105: 335-348, 2013, doi: 10.1016/j.apenergy.2012.12.061.
37. De Bellis, V., Bozza, F., Tufano, D., "A Comparison Between Two Phenomenological Combustion Models Applied to Different SI Engines," SAE Technical Paper 2017-01-2184, 2017, doi: 10.4271/2017-01-2184.
38. Bozza, F., De Bellis, V., Giannattasio, P., Teodosio, L. et al., "Extension and Validation of a 1D Model Applied to the Analysis of a Water Injected Turbocharged Spark Ignited Engine at High Loads and over a WLTP Driving Cycle," *SAE Int. J. Engines* 10(4):2141-2153, 2017, doi: 10.4271/2017-24-0014.
39. Gatowsky, J., Heywood, J., "Flame Photographs in a Spark-Ignition Engine," *Combustion and Flame* 56:71-81, 1984, doi: 10.1016/0010-2180(84)90006-3.
40. Gouldin, F., "An application of Fractals to Modeling Premixed Turbulent Flames," *Combustion and Flame* 68(3):249-266, 1987, doi:10.1016/0010-2180(87)90003-4.
41. De Bellis, V., Bozza, F., Fontanesi, S., Severi, E. et al., "Development of a Phenomenological Turbulence Model through a Hierarchical 1D/3D Approach Applied to a VVA Turbocharged Engine," *SAE Int. J. Engines* 9(1):506-519, 2016, doi:10.4271/2016-01-0545.
42. Bozza, F., Teodosio, L., De Bellis, V., Fontanesi, S. et al., "Refinement of a 0D Turbulence Model to Predict Tumble and Turbulent Intensity in SI Engines. Part II: Model Concept, Validation and Discussion," SAE Technical Paper 2018-01-0856, 2018, doi: 10.4271/2018-01-0856.
43. Bozza, F., De Bellis, V., and Teodosio, L., "A Tabulated-Chemistry Approach Applied to a Quasi-Dimensional Combustion Model for a Fast and Accurate Knock Prediction in Spark-Ignition Engines," SAE Technical Paper 2019-01-0471, 2019, doi: 10.4271/2019-01-0471.
44. Andrae, J., Kovács, T., "Evaluation of Adding an Olefin to Mixtures of Primary Reference Fuels and Toluene to Model the Oxidation of a Fully Blended Gasoline," *Energy & Fuels*, 30(9), 7721-7730, 2016, doi: 10.1021/acs.energyfuels.6b01193.
45. Lavoie, G., Heywood, J., Keck, J., "Experimental and theoretical study of nitric oxide formation in internal combustion engines," *Combustion science and technology* 1(4): 313–326, 1970, doi: 10.1080/00102206908952211.
46. Arsie, I, Pianese, C.; Rizzo, G., "Models for the prediction of performance and emissions in a spark ignition engine - A sequentially structured approach," SAE Technical Paper 980779, 1998, doi: 10.4271/980779.
47. Kaplan, J., Heywood, J., "Modeling the spark ignition engine warm-up process to predict component temperatures and hydrocarbon emissions," SAE Technical Paper 1991, 361-376, doi: 10.4271/910302.
48. Lavoie, G., "Correlations of combustion data for SI Engine calculations–laminar flame speed, quench distance and global reaction rates," SAE Technical Paper1978,1015-1033, doi: 10.4271/780229.
49. Schramm, J., Sorenson, S., "A model for hydrocarbon emissions from SI engines," SAE Technical Paper 1990, 2331-2349, doi: 10.4271/902169.
50. North, G., Santavicca, D., "The fractal nature of premixed turbulent flames," *Combustion Science and Technology* 72(4-6): 215-232, 1990, doi: 10.1080/00102209008951648.
51. Rigoni, E., Poles, S., "NBI and MOGA-II, two complementary algorithms for multiobjective optimization," presented at Dagstuhl Seminar Proceedings IBFI, Germany, 2005.
52. Coello, C., van Veldhuizen, D., Lamont, G., "Evolutionary Algorithms for Solving Multi-Objective Problems," (Springer US, 2007), 24-55, doi: 10.1007/978-0-387-36797-2.

Acronyms

0D-1D-3D	Zero-One-Three-dimensional
AFTDC	After firing top dead center
AI	Auto-Ignition
BDC	Bottom dead center
BMEP	Brake mean effective pressure
BSFC	Brake specific fuel consumption
CAD	Crank angle degree
CFD	Computational fluid dynamic
CLD	Chemi-luminescence detector
CR	Compression ratio
DoE	Design of Experiment
EA	Evolutionary algorithms
EGR	Exhaust gas recirculation
EVC	Exhaust valve closure
FID	Flame ionization detector
ICE	Internal combustion engine
IMEP	Indicated mean effective pressure
IRD	Infra-red detector
IVO	Intake valve opening
LFS	Laminar flame speed
MFB	Mass fraction burned
PFI	Port fuel injection
PMEP	Pumping mean effective pressure
RANS	Reynolds averaged Navier-Stokes
RDE	Real driving emission
RMSD	Root-mean-square deviation
RNG	Renormalization group
SI	Spark ignition
TDC	Top dead center
TWC	Three-way catalyst
VVA	Variable valve actuation
VVT	Variable valve timing
WOT	Wide open throttle

Symbols

A	Flame front area
c_{trans}	Laminar-turbulent transition multiplier
c_{wrk}	Flame wrinkling multiplier
D_3	Flame front fractal dimension
k	Turbulent kinetic energy
S_L	Laminar flame speed
x_r	Residual mass fraction at intake valve closing
x_{wc}	Wall-combustion tuning constant

Subscripts

0/10/50/90	Referred to 0/10/50/90% of MFB
b	Burned
L	Laminar
MAX	Related to maximum level
MIN	Related to minimum level
T	Turbulent
u	Unburned

Greeks

Γ	Scale of flame front wrinkling
ε	Dissipation rate
λ	Relative air/fuel ratio
ρ	Density